Structural, Dielectric, and Rheological Characterization of a Thermotropic Polyester Displaying Smectic A, Nematic, and Isotropic Phases

Douglass S. Kalika,*,† Man-Ruo Shen, Xiao-Ming Yu, and Morton M. Denn*

Center for Advanced Materials, Lawrence Berkeley Laboratory, and Department of Chemical Engineering, University of California, Berkeley, California 94720

Pio Iannelli, Norberto Masciocchi, Do Y. Yoon,* and William Parrish

IBM Almaden Research Center, 650 Harry Road, San Jose, California 95120

C. Friedrich and C. Noël

Laboratoire de Physicochimie Structurale et Macromolèculaire, ESPCI, 10 Rue Vauquelin, 75231 Paris, Cedex 05, France

Received August 9, 1989

ABSTRACT: We report structural, dielectric, and rheological properties of a thermotropic liquid-crystalline polyester, which exhibits a crystal–crystal transition at 137 °C and crystal-to-smectic A, smectic A-to-nematic, and nematic-to-isotropic transitions at 164, 180, and 220 °C, respectively; initial phase identifications were made by using optical microscopy techniques and confirmed by X-ray diffraction measurements. The dielectric results are highly sensitive to phase state, particularly at the lower frequencies investigated, where interfacial polarization effects dominate due to the broad biphasic regions present in our samples. Higher frequency measurements indicate a sizable increase in dipolar (rotational) mobility at the crystal–crystal transition, no change in the dielectric constant (ϵ') at the crystal-to-smectic A transition, and a decrease in ϵ' at the onset of the nematic phase. In contrast to the dielectric results, dynamic rheological measurements are insensitive to the crystal–crystal transition, but large, nearly stepwise decreases in complex viscosity are observed across both the crystal-to-smectic A and smectic A-to-nematic transitions, with a slight increase encountered at the onset of isotropy. Constant-temperature frequency sweeps recorded for the smectic A phase indicate a persistent shear thinning behavior, with the storage modulus (G') greater than the loss modulus (G'') over the investigated frequency range. Steady shear viscosity measurements obtained during cooling are consistent with the dynamic results and indicate that the layering of the smectic A phase is apparently not disrupted by steady shearing at low rates. A lack of reversibility is observed for the rheological measurements carried out from 230 °C relative to those initiated at 190 °C; this may be the result of transesterification reactions occurring at the higher temperature.

Introduction

Since the initial development of thermotropic liquid-crystalline polymers, a large number of structures have been reported that produce at least one mesophase in the melt.[1-4] These polymers are comprised of a wide variety of rigid and flexible components, combined into both main-chain and side-chain structures. Studies of structure–property relationships for these materials have typically correlated the observed thermal transitions and mesophase behavior with chemical structural aspects such as length of flexible spacer, substitution on the mesogenic core, introduction of kinked segments, etc. Despite this high level of synthetic activity, rheological characterizations for thermotropic liquid-crystalline polymers have been limited to only a few materials, most notably the main-chain copolymers composed of *p*-hydroxybenzoic acid (HBA)/poly(ethylene terephthalate) (PET)[5-7] and *p*-hydroxybenzoic acid (HBA)/2,6-hydroxynaphthoic acid (HNA).[8-11] The primary reason for this limited scope of rheological study is sample quantity; while both the HBA/PET and HBA/HNA copolymers have been produced on a large scale, most liquid-crystalline polymer syntheses do not generate sufficient quantities for melt rheology experiments. The commercially available materials display only nematic order in the melt and decompose with increasing temperature prior to any well-established clearing transition. Only a few studies have appeared that follow the rheological properties of a thermotropic polymer through a mesophase transition. It was the objective of this work to rheologically characterize a thermotropic liquid-crystalline polymer that displays both a smectic-to-nematic and a nematic-to-isotropic transition with increasing temperature. Specifically, a material originally described by Galli et al.[12] was synthesized in sufficient quantity for torsional rheological measurements. Thermal transitions and phase identifications were established by a combination of differential scanning calorimetry (DSC), optical microscopy, and X-ray diffraction. In addition, dielectric measurements were performed on the material in order to assess high-frequency dipolar rotational mobility across the observed phase transitions.

Background

Rheology. Most of the data available on the rheological behavior of liquid-crystalline materials through well-defined nematic-to-isotropic clearing transitions comes from studies on either low molecular weight liquid crystals[13] or lyotropic (solution-based) liquid-crystalline polymers.[14,15] In both cases, a sharp increase in shear viscosity is observed at the first appearance of the isotropic phase with either increasing temperature or decreasing solute concentration. This behavior has been confirmed for thermotropic polymers as well. Wissbrun and Griffin,[16] for example, measured the rheological properties of a main-chain polyester with flexible spacer modification in torsional flow

† Present address: Department of Chemical Engineering, University of Kentucky, Lexington, KY 40506.

0024-9297/90/2223-5192$02.50/0

above and below the nematic-to-isotropic transition temperature. In spite of the higher temperature, the isotropic phase (240 °C) showed a consistently higher melt viscosity than the nematic phase (210 °C). In addition, dynamic-viscosity frequency sweeps showed strong shear thinning across the entire frequency range for the nematic case, while the isotropic material displayed virtually no shear thinning. Results of Blumstein and co-workers[17] reported for two nematic polyesters based on 4,4′-dihydroxy-2,2′-dimethylazoxybenzene and alkanedioic acids were consistent with those of Wissbrun and Griffin. These materials displayed a significant increase in measured complex viscosity at the nematic-to-isotropic transition; the negative viscosity–temperature dependence of the isotropic phase created a relative maximum in viscosity. This work was extended by Kumar et al.[18] to include members of the series with longer flexible spacers, for which a smectic-to-isotropic transition was observed (see below).

Although a distinct nematic-to-isotropic transition is not observed prior to thermal degradation for the HBA/PET copolymer, a recent study by Amundson and co-workers[19] has assessed the influence of increasing nematic fraction on the measured viscosity of 60/40 HBA/PET. The copolymer is biphasic at this composition, containing both nematic and isotropic fractions, and the relative amount of nematic phase present can be increased by solid-phase polymerization. Dynamic rheological results show an overall decrease in complex viscosity with increasing nematic fraction, consistent with the observations described above.

Relatively few studies have appeared in the literature addressing the possible rheological effects of other mesophase transitions, specifically smectic-to-nematic or smectic-to-isotropic transitions. Qualitatively, a layered smectic phase would be expected to have a higher viscosity than a nematic phase under comparable conditions, as the lateral interactions that create the smectic layering will also produce increased resistance to flow. In the work of Kumar et al.[18] noted above, it was discovered that incorporating an alkane flexible spacer of length $n = 18$ into the polymer structure produces a smectic C mesophase. Dynamic rheological studies on this material indicate a sharp increase in the measured complex viscosity upon cooling through the isotropic-to-smectic C transition, in contrast to the results for samples with shorter flexible spacer lengths, for which only a nematic mesophase was observed. These data appear to represent the first rheological characterization of a smectic liquid-crystalline polymer.

Dielectric Measurements. Dielectric characterizations of thermotropic liquid-crystalline polymer systems have been reported for both main-chain and side-chain materials. The main-chain studies have focused on the HBA/PET[20,21] and HBA/HNA[22,23] copolymers. Multiple dielectric losses are observed in both cases, corresponding to the glass transition and localized rotations about the polymer chain. By appropriate variation of the copolymer compositions, these localized motions can be correlated with specific copolymer components. For the case of HBA/HNA, the observed total dielectric increment, $\Delta\epsilon$, is found to be significantly lower than is predicted by dipole calculations based on full mobility for the polymer chain segments.[23] This reduced response is most likely due to the conformational constraints that result in very small net dipole moments.[32] A wealth of dielectric literature has evolved on polyacrylate and polysiloxane side-chain polymers displaying both nematic and smectic mesophases in the melt; these results have recently been reviewed by Monnerie and co-workers.[24]

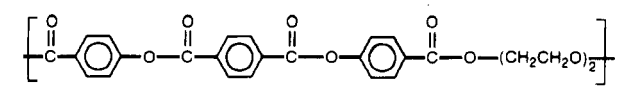

Figure 1. Thermotropic liquid-crystalline polymer synthesized according to the methods of Galli et al.[12]

Experimental Methods

Synthesis. The polymer was synthesized according to the methods of Galli et al.;[12] it consists of a triad aromatic mesogenic segment and a diethylene glycol flexible spacer (Figure 1). Approximately 10 g was prepared. Chemical characterization was achieved by using ^{1}H NMR spectroscopy under ambient conditions, with trifluoroacetic acid (TFA) as the solvent. The relative molecular weight of the sample was established by intrinsic viscosity measurements.

Differential Scanning Calorimetry. Thermal transition characteristics were established by using differential scanning calorimetry (DSC), with heating and cooling cycles carried out in a Du Pont 910 differential scanning calorimeter under an inert atmosphere. Sample size was typically 10 mg, with runs performed at rates of 10 and 20 °C/min.

Optical Microscopy. Sample textures were examined at various temperatures under crossed polarizers by using an Olympus BHA-P polarizing microscope equipped with a Mettler FP5 hot stage; initial phase identification was accomplished by analogy to textures observed for well-characterized low molecular weight liquid crystals and liquid-crystalline polymers. Heating/cooling rates in the range of the phase transitions were 2–3 °C/min.

X-ray Diffraction. The polymer powder samples were prepared on thin silicon single-crystal wafers with surfaces cut parallel to the (510) plane; silicone grease was used as a binder. The X-ray intensity data were collected over a range of temperatures on a vertical-scanning-type powder diffractometer operating in a standard θ–2θ geometry.[25] A copper target long-line focus tube was operated at 50 kV and 20 mA. Beam collimation was controlled with a 0.5° entrance slit to define the primary beam, an antiscatter slit, and a 0.12° receiving slit in the diffracted beam. Vertical divergence was limited by Soller slits with a 4° aperture placed in the incident beam. A curved graphite monochromator was placed after the receiving slit to reflect only Cu Kα radiation. The recorded diffraction patterns ranged from 1.6° to 36.6° (2θ); at lower angles the primary beam interfered with the measurement of d-spacings larger than about 35 Å. A Na(Tl)I scintillation counter with pulse amplitude discrimination was used.

Automated step-scan collection and recording was controlled with an IBM PC/AT personal computer, allowing selection of the scan range, step increment, and count time. Recorded data were transferred to a host computer (IBM 3090) for analysis. The peak position (2θ) and intensity was determined by the cubic first derivative method.[26]

The specimen was heated from below by clamping the silicon (510) wafer to a flat silicon nitride plate containing an electric heating element.[27] A cylindrical heat shield with long beryllium window fit over the heater, and an outer vacuum-tight chamber with a Mylar window covered the assembly. The specimen temperature was measured by a chromel–alumel thermocouple and maintained by a digital temperature controller. Two external thermocouples were used to check the uniformity of the temperature distribution on the specimen area and to ensure consistency between the specimen temperature and the set-point temperature. The diffraction experiments were performed under low vacuum (0.5 Torr) in order to avoid air scatter and absorption losses and to prevent possible oxidation of the specimen.

Dielectric Measurements. Dielectric characteristics of the polymer were established over a wide range of temperatures using the Hewlett-Packard Model 4275A multifrequency LCR meter. The frequency range for these measurements was 10 kHz to 10 MHz, with a test amplitude of 1 V. Sample films were prepared by squeezing the polymer between glass slides at 190 °C, using 50-μm Kapton spacers to ensure uniform sample thickness; the

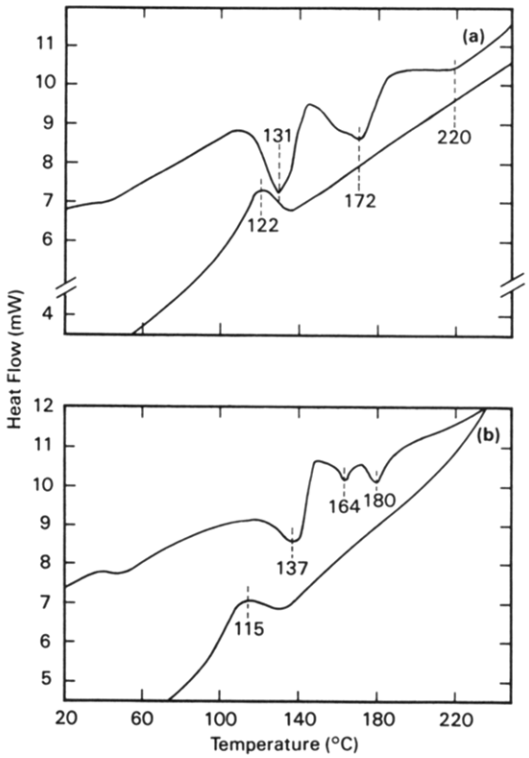

Figure 2. Differential scanning calorimetry (DSC) traces, 10 °C/min: (a) first heating/cooling; (b) second heating/cooling.

electrode diameter was 10 mm. Heating sweeps were performed over the range 20–240 °C at a rate of 2 °C/min.

Rheology. Dynamic and steady shear rheological measurements were performed on a Rheometrics mechanical spectrometer Model 705 in the parallel-plate arrangement (25-mm platens). Each sample was dried for 24 h [60 °C, (<1 mmHg)] prior to measurement to remove moisture and loaded into the rheometer in powder form at test temperature under a nitrogen atmosphere. The parallel-plate gap spacing was typically 0.50 mm and was adjusted with temperature in order to compensate for thermal expansion/contraction of the rheometer platens. Dynamic strain amplitudes were varied from 2 to 20% with increasing temperature to achieve sufficient levels of transducer torque for all measurements.

Results

Phase Behavior. The phase behavior of the polymer was established by differential scanning calorimetry (DSC) and optical microscopy. Consecutive DSC sweeps for the as-synthesized material (10 °C/min) are shown in Figure 2. In the first heating (Figure 2a), a base-line shift is evident at approximately 35 °C, in addition to three endotherms at 131, 172 (with a shoulder at 162 °C), and 220 °C. Upon cooling, a single exothermic transition is observed at 122 °C. In the second heating (Figure 2b), the transitions are shifted to higher temperatures (T = 137, 164, and 180 °C); the endotherm that was previously centered at 172 °C is now separated into two distinct features. Also, an exotherm is evident in the temperature range 145–160 °C. Upon cooling, the observed exothermic transition is shifted to lower temperature, approximately 115 °C. Curves recorded at a scanning rate of 20 °C/min were consistent with those discussed above, and further heating and cooling cycles had only a marginal effect on the recorded curves.

For the optical observations, a small amount of polymer was placed between glass plates and heated initially to 120 °C at 20 °C/min; subsequent heating (to 250 °C) and cooling was performed at a rate of 2–3 °C/min. Below 150 °C, the material displays a very high viscosity and no typical texture can be induced. At and above 150 °C, oily streaks are evident, which indicate the appearance of a smectic A phase. Simultaneously, the thin portions of the preparation become black, the mesogenic groups aligning with an average orientation perpendicular to the glass surfaces. Such a homeotropic alignment is typical of uniaxial phases (S_e, S_b, S_a, N). The homeotropic texture of the smectic A phase can be distinguished from that of the nematic phase in this case by touching the cover glass, at which point oily streaks and very small focal conics are observed. Over the temperature range 150–170 °C, the viscosity decreases markedly and the ill-defined texture is progressively replaced by the smectic A texture. From 170 to 185 °C no significant change occurs (Figure 3).

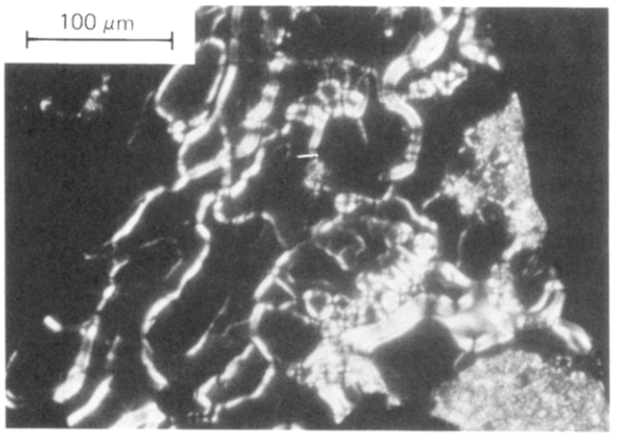

Figure 3. Photomicrograph taken under crossed polarizers of liquid-crystalline polymer displaying oily streaks and dark homeotropic regions (smectic A texture); 177 °C.

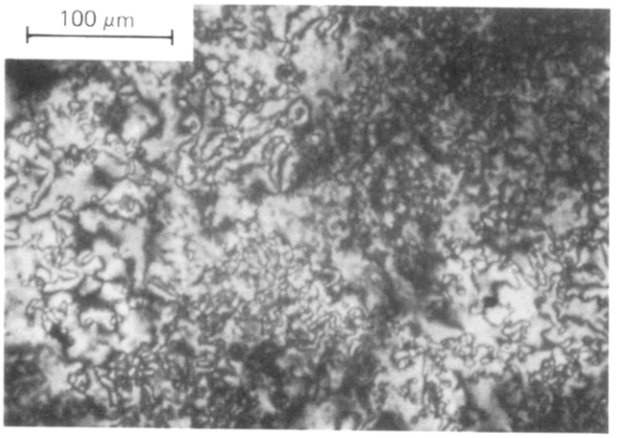

Figure 4. Photomicrograph taken under crossed polarizers of liquid-crystalline polymer displaying a schlieren texture; 215 °C.

In the temperature range 185–190 °C, a second decrease in viscosity is evident as the nematic phase appears: the oily streaks disappear and the small focal conics are replaced by threads. The homeotropic regions become extremely birefringent when the cover glass is touched, and at higher temperature (approximately 200 °C) it is possible to observe a schlieren texture. At approximately 210 °C, the first drops of isotropic liquid appear, and by 250 °C, all of the material is in the isotropic state.

Upon cooling, nematic droplets evolve (225–215 °C) that grow and coalesce to form large domains, which exhibit the unmistakable schlieren texture (Figure 4). As the temperature is further decreased, the homeotropic texture progressively replaces the schlieren texture, and in the range 170–160 °C oily streaks appear, characteristic of the smectic A phase. A chevron or striated texture can also

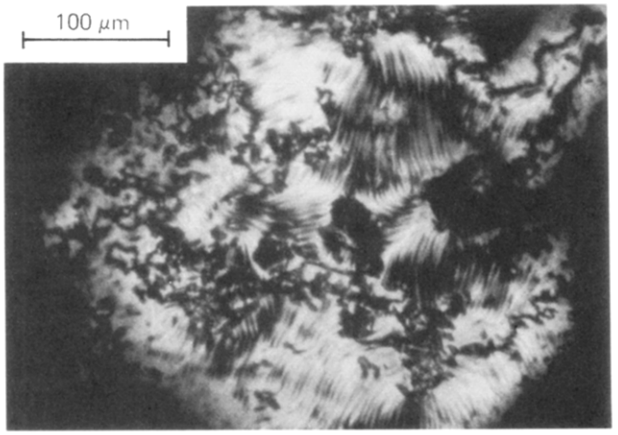

Figure 5. Photomicrograph taken under crossed polarizers of liquid-crystalline polymer displaying a chevron texture; 145 °C.

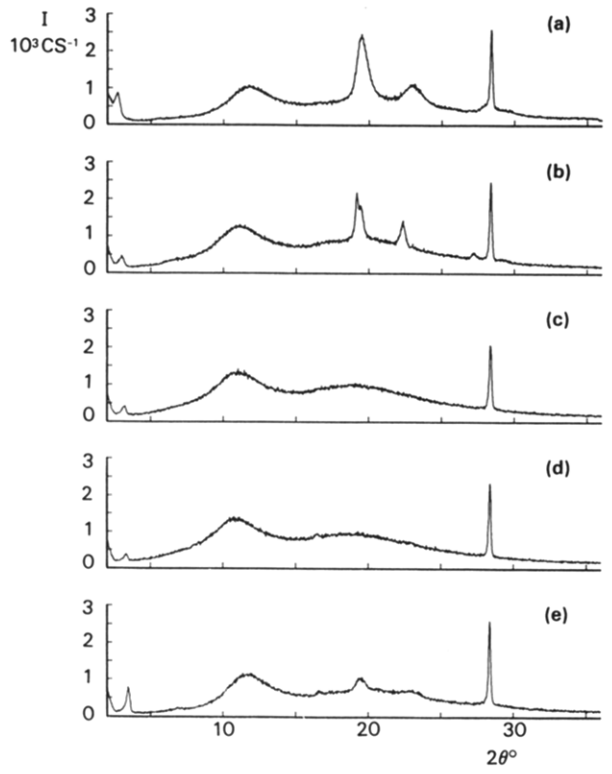

Figure 6. X-ray diffraction plots of intensity (counts/s) versus peak position (2θ°, first heating): (a) initial room-temperature pattern (25 °C); (b) 150 °C; (c) 180 °C; (d) 200 °C; (e) room-temperature pattern (25 °C) recorded after heating to 230 °C.

be observed in this temperature range (Figure 5); this texture typically appears just below a nematic-to-smectic A transition. It should be noted that, because of the extent of the transition temperature ranges, it is virtually impossible to obtain monophasic systems. Depending on the temperature at which the microscopic observations are made, solid/S_a, solid/S_a/N, S_a/N, or N/I mixtures are formed.

X-ray Diffraction. The initial room-temperature diffraction pattern for the polymer is shown in Figure 6a. The narrow peak at 2.72° (2θ), d = 32.50 Å, is assumed to be the (001) reflection. Additional reflections are observed at 19.50° (4.55 Å) and 23.02° (3.86 Å); the broad feature at approximately 12° and the sharp peak at 28.4° are due to the silicone grease binder and trace silicon powder 640B (used as a reference), respectively (see Table Ia). Room-temperature patterns recorded with an alternate binder (5.0% collodion in amyl acetate) that did not

Table I
X-ray Diffraction Results (Peak Positions (2θ°) and d-Spacing (Å)) for the Two Crystalline Phases Observed at (a) 25 and (b) 150 °C, Respectively (First Heating)

	T, °C	2θ, deg	d-spacing, Å
a	25	2.72	32.48
		19.49	4.55
		23.03	3.86
b	150	3.00	29.45
		19.18	4.63
		22.34	3.98
		27.23	3.27

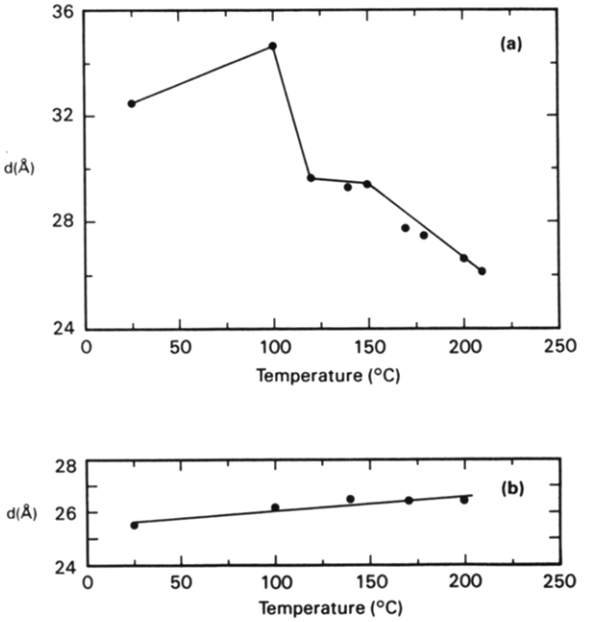

Figure 7. d-spacing (Å) of the (001) reflection as a function of temperature: (a) first heating; (b) second heating.

produce the broad background at 12° displayed an additional peak at approximately 5.4° (16.3 Å), which confirms the assignment of the narrow low-angle peak to the base reflection (001). This latter binder was found to have a degradative effect on the polymer at higher temperatures, however, and its use was discontinued.

The polymer was heated stepwise from 25 °C with diffraction patterns recorded at temperatures up to 230 °C (first heating) and 260 °C (second heating); approximately 30 min was necessary for each scan after the establishment of thermal equilibrium. At 100 °C, the pattern is qualitatively similar to the room-temperature result, with the (001) d-spacing increasing to 34.64 Å due to thermal expansion and a small peak appearing at 27.50° (3.24 Å) which is present as a shoulder on the silicon reference reflection at room temperature. At 120 °C, the (001) reflection is shifted to *higher* angles (d = 29.64 Å; see Figure 7a), and this shift is accompanied by a marked decrease in the (001) reflection intensity. In the temperature range 120–150 °C, the higher angle peaks narrow somewhat, but the (001) reflection remains essentially unchanged (Figure 6b; Table Ib). Between 150 and 170 °C, the intensity of the higher angle peaks drops dramatically, and by 180 °C these peaks disappear completely (Figure 6c), leaving only a diffuse halo at higher angles. Careful examination of the pattern recorded at 200 °C (Figure 6d) shows the appearance of two very weak higher angle reflections at 16.46° (5.38 Å) and 22.90° (3.88 Å): these reflections disappear above 210 °C but reemerge on cooling. The (001) reflection shifts to progressively higher angles over this temperature range and gradually

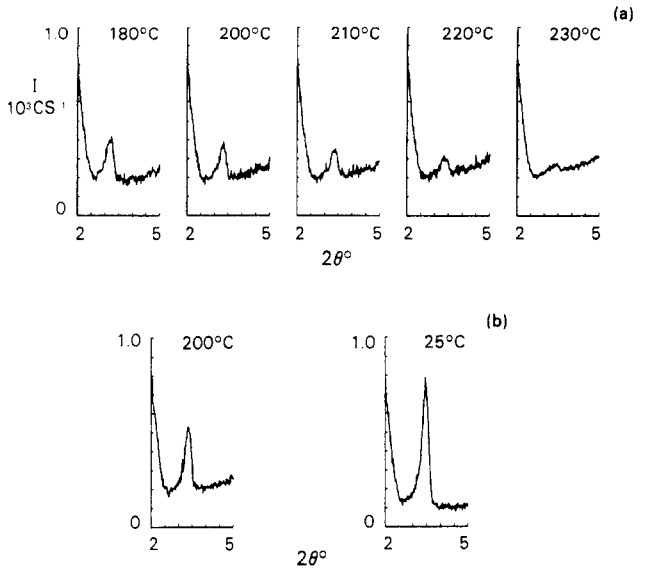

Figure 8. X-ray diffraction plots of intensity (counts/s) versus peak position ($2\theta°$) in the range of the (001) reflection: (a) first heating, 180–230 °C; (b) cooling.

broadens and weakens in intensity until its virtual disappearance at 230 °C (Figure 8a).

Upon cooling, diffraction patterns were recorded at 200, 160, and 25 °C. The (001) reflection reemerges by 200 °C (Figure 8b), but the higher angle peaks are only seen at room temperature (Figure 6e). The room-temperature scan shows the intensity of the higher angle peaks as greatly reduced compared to the initial (as-synthesized) result (Figure 6a) and the (001) reflection at 3.46° (d = 25.53 Å). Subsequent annealing experiments on a separate sample revealed that the intensity of the higher angle peaks could be increased dramatically by holding the polymer at 150 °C.

The measured (001) d-spacing as a function of temperature for the second heating cycle is detailed in Figure 7b. In contrast to the first heating, the characteristics of the (001) reflection peak remain essentially constant up to 170 °C, with a small increase in d-spacing reflecting the thermal expansion of the material. Above 170 °C the higher angle peaks disappear, and the intensity of the (001) peak decreases gradually until its disappearance at 230 °C. Cooling from 260 °C shows a complete recovery of the various features.

Dielectric Measurements. The dielectric results for the polymer are comprised of a single heating sweep from 20 to 240 °C at a rate of 2 °C/min; the sample was prepared at 190 °C and cooled slowly to room temperature prior to measurement. A plot of dielectric constant (ϵ') versus temperature for all frequencies is provided in Figure 9a. The lower frequency data (10–400 kHz) display a dramatic increase in ϵ' above 50 °C with relative maxima at approximately 145 and 205 °C; the accompanying dielectric loss values over this range are extremely large ($\epsilon'' \sim$ O(100)). The higher frequency data (1–10 MHz) show an incremental increase in ϵ' between 20 and 130 °C ($\Delta\epsilon'$ = 2.5 (1 MHz)) and are then independent of temperature in the range 130–190 °C (see expanded plot, Figure 9b). Above 190 °C, ϵ' drops sharply, with a small recovery at 225 °C creating a relative maximum.

Rheology. Initial rheological measurements were accompanied by loading the polymer powder into the mechanical spectrometer at 190 °C under a nitrogen atmosphere; dynamic data (frequency = 1, 10 rad/s) were recorded over heating and cooling sweeps at 5 °C intervals.

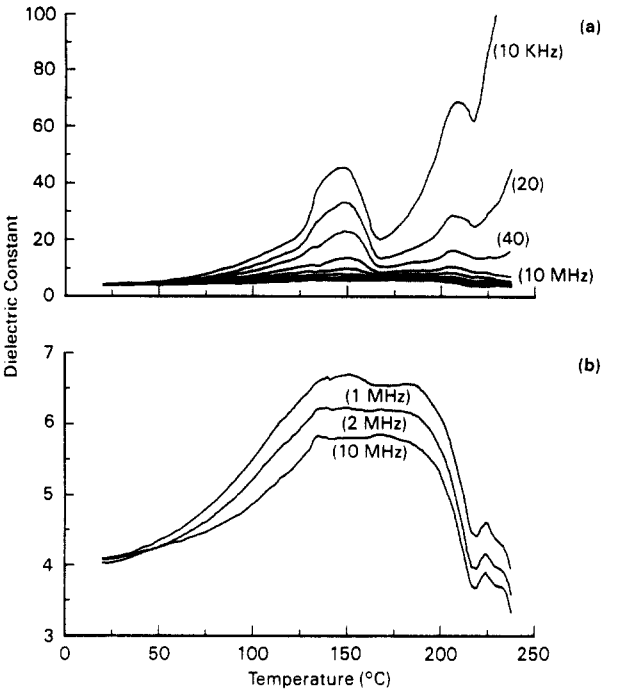

Figure 9. Dielectric constant (ϵ') versus temperature: (a) frequencies of 10 kHz to 10 MHz; (b) frequencies of 1, 2, and 10 MHz (expanded scale).

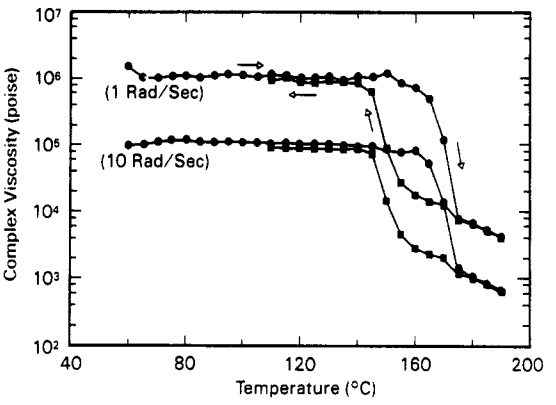

Figure 10. Magnitude of the complex viscosity ($|\eta^*|$, P) versus temperature, cycling to 190 °C, at 1 and 10 rad/s. Sample loaded at 190 °C (heating = ●, cooling = ■).

The results from a typical heating and cooling cycle are provided in Figure 10; the material was loaded at 190 °C and cooled to 60 °C over 30 min. Rheological data were then recorded at heating and cooling rates of 1.25 °C/min. For the range 60–160 °C, the magnitude of the complex viscosity ($|\eta^*|$) is nearly constant. A dramatic drop in viscosity is observed from 160 to 175 °C, followed by a more gradual decrease with increasing temperature; the measured viscosity activation energy across the range 175–190 °C is approximately 42 kJ/mol. The cooling results for the same sample are superimposed on the heating data. Excellent agreement is observed, with supercooling accounting for the offset of 20 °C in the region of steepest increase.

A heating sweep that extends to higher temperatures is shown in Figure 11; the polymer was loaded at 190 °C and then cooled to 100 °C prior to measurement. Across the range 100–190 °C, the viscosity data (Figure 11a) are essentially identical with those provided in Figure 10, with an additional decrease in the magnitude of the complex viscosity encountered from 190 to 220 °C. A subsequent increase in viscosity creates a relative minimum at 220 °C. Figure 11b provides the corresponding dynamic moduli

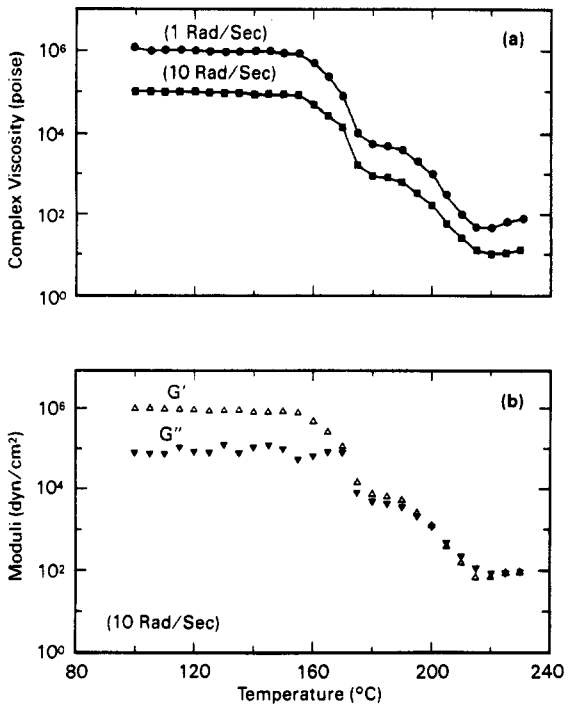

Figure 11. (a) Magnitude of the complex viscosity ($|\eta^*|$, P) versus temperature, heating to 230 °C, at 1 and 10 rad/s. (b) Storage modulus (G', dyn/cm²) and loss modulus (G'', dyn/cm²) versus temperature, heating to 230 °C, at 10 rad/s. Sample loaded at 190 °C (η^*(1 rad/s) = ●, η^*(10 rad/s) = ■, G' = Δ, G'' = ▼).

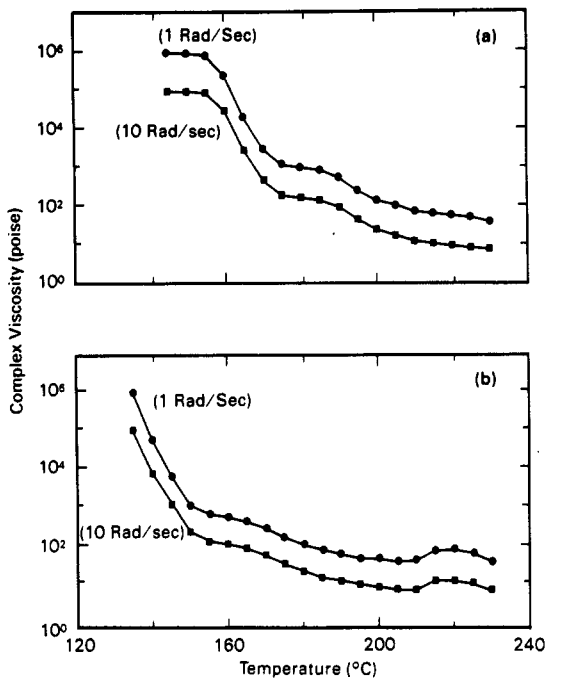

Figure 12. Magnitude of the complex viscosity ($|\eta^*|$, P) versus temperature at 1 and 10 rad/s. Sample loaded at 230 °C: (a) heating; (b) cooling (η^*(1 rad/s) = ●, η^*(10 rad/s) = ■).

for this sample (10 rad/s). In the range 100–160 °C the storage modulus (G') is approximately 1 order of magnitude larger than the loss modulus (G''); the scatter in G'' reflects the sensitivity limits of the rheometer. Both moduli drop across the range 160–175 °C, but the storage modulus continues to dominate until approximately 200 °C, where the two values are of comparable magnitude.

In Figure 12, two separate temperature sweeps are presented in which the polymer was loaded into the rheometer at 230 °C. In the first case (Figure 12a), the sample was loaded at 230 °C and cooled immediately to 140 °C,

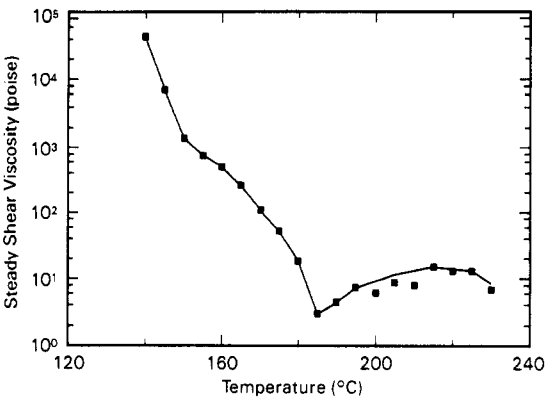

Figure 13. Steady shear viscosity (P) versus temperature during cooling at 0.5 s^{-1}. Sample loaded at 230 °C.

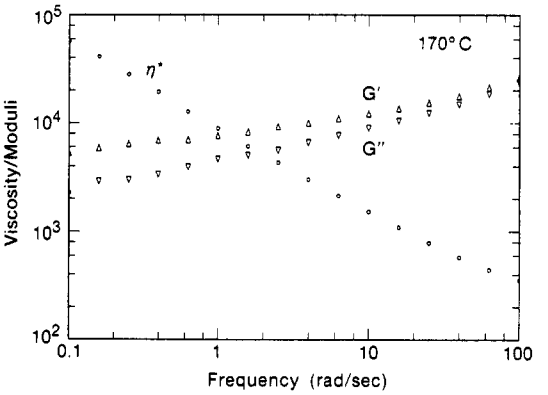

Figure 14. Magnitude of the complex viscosity ($|\eta^*|$, P), storage modulus (G', dyn/cm²), loss modulus (G'', dyn/cm²) versus frequency (rad/s) at 170 °C (η^* = ○, G' = Δ, G'' = ▽).

and dynamic data were recorded from 145 to 230 °C at a heating rate of 1.25 °C/min. In the second case (Figure 12b), the sample was loaded at 230 °C and dynamic data were recorded directly over a cooling rate of −1.25 °C/min. The features of these data are similar to those discussed above (sample loaded at 190 °C), but the complex viscosity values measured in the intermediate temperature range (175–190 °C) are significantly lower for this case. This has the effect of reducing the magnitude of the second decrease in viscosity (190–220 °C) and increasing the magnitude of the first decrease in viscosity (155–175 °C). A steady shear cooling sweep with a similar thermal history (230–140 °C) was recorded at a shear rate of 0.5 s^{-1}, and these data are provided in Figure 13.

Constant-temperature frequency sweeps (0.1–100 rad/s) were also performed for a sample loaded at 190 °C and then cooled; measurements were performed at 170, 150, and 140 °C. The data recorded at 170 °C (Figure 14) indicate a highly shear thinning material, with the complex viscosity–frequency curves displaying a slight upward concavity and G' and G'' of comparable magnitude, with G' somewhat greater. The data recorded at 140 and 150 °C (Figure 15) show a solidlike behavior, with the storage modulus essentially independent of both frequency and temperature: G' is approximately 1 order of magnitude greater than G'' in this temperature range (refer to Figure 11b).

Discussion

Phase Behavior. The results of the DSC and optical microscopy studies, in conjunction with the X-ray diffraction experiments, form a coherent picture for the phase behavior of this thermotropic liquid-crystalline polymer. The DSC sweeps indicate an apparent crystal-

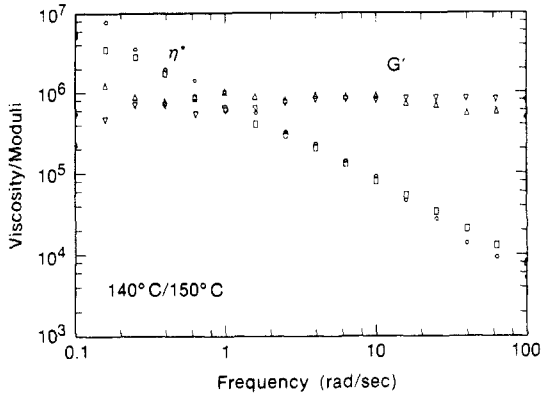

Figure 15. Magnitude of the complex viscosity ($|\eta^*|$, P), storage modulus (G', dyn/cm²) versus frequency (rad/s) at 140 and 150 °C (η^*(140 °C) = ○, η^*(150 °C) = □, G'(140 °C) = △, G'(150 °C) = ▽).

crystal (or crystal-to-higher order smectic) transition at 137 °C, a crystal-to-smectic A transition at 167 °C, a smectic A-to-nematic transition at 180 °C, and an isotropic clearing at approximately 220 °C; the mesophase identifications were initially made using optical microscopy and confirmed during the course of the X-ray experiments (see below). Galli et al.[12] reported the phase transitions of this polymer as follows: crystal-to-smectic transition at 185 °C, smectic-to-nematic transition at 222 °C, and nematic-to-isotropic transition at 288 °C. The somewhat lower transition temperatures observed in the present case may be a reflection of a lower degree of polymerization. Dilute-solution viscosity measurements for the present material indicate an intrinsic viscosity of 0.12 dL/g (TFA, 25 °C) as compared with the value of 0.23 dL/g reported by Galli and co-workers.[12] In addition, no crystal–crystal transition was observed in the original work, as compared with the sizable DSC enthalpy observed here at 137 °C (second heating). Bilibin et al.[28] synthesized a higher molecular weight sample of this same polymer ($[\eta]$ = 0.60 dL/g) and reported a crystal-to-nematic transition at 198 °C and an isotropic clearing at 335 °C; no smectic mesophases were observed.

The initial room-temperature X-ray diffraction results (Figure 6a) indicate considerable crystallinity and a well-defined periodicity along the chain axis. Heating to the range of the first DSC endotherm produces a dramatic decrease in the measured (001) d-spacing (refer to Figure 7a), with the higher angle peaks shifting only slightly. This result, combined with the failure to obtain any significant optical texture in this range, is consistent with the occurrence of a crystal–crystal transition, across which the molecules reorganize into a smaller stacking period; note also the *exotherm* present in the DSC heating sweeps at approximately 145 °C, which suggests a recrystallization. Above 150 °C, the higher angle crystalline peaks decrease in intensity and disappear completely by 180 °C (Figure 6c), at which temperature they are replaced by a diffuse halo centered on a spacing of approximately 4.55 Å; the position of the halo corresponds to the average lateral approach distance of the mesogenic cores. This result agrees with the occurrence of the crystal-to-smectic A transition (DSC endotherm centered at 172 °C, first heating). Over this temperature range (>150 °C), the (001) d-spacing again decreases and continues to do so until the reflection peak disappears at 230 °C, indicating a progressive reduction of the order parameter. The temperature of the smectic A-to-nematic transition, which DSC and optical microscopy place between 180 and 190 °C, is difficult to establish based on the X-ray diffraction results. Examination of the (001) reflection over the range 180–230 °C (Figure 8a) shows only a gradual broadening and decrease in the intensity of the peak, consistent with the progression smectic → nematic → isotropic; no distinct stepwise change in the peak appearance is observed over the 10 °C measurement intervals. This issue is complicated further by the faint higher angle reflections present in the range 180–210 °C (see Figure 6d). These peaks suggest the possible presence of a very small amount of higher order smectic material.

The limited number of diffraction patterns recorded upon cooling from 230 °C indicates the reversible reappearance of the (001) reflection by 200 °C, supercooling of the crystalline phase below at least 160 °C (the DSC crystallization exotherm is located at 122 °C), and a significantly smaller (001) d-spacing at room temperature compared to the as-synthesized material (25.53 Å vs 32.50 Å); this d-spacing value agrees reasonably well with the estimated monomeric repeat distance for the material of 27.7 Å (all-trans configuration).[29] Upon second heating, the development of the diffraction patterns is qualitatively similar to that of the first heating, with the exception of the (001) peak position. The (001) d-spacing shows only a small increase with temperature (Figure 7b) in contrast to the sizable changes observed over the first heating. This is surprising considering the similarity of the first and second DSC heating sweeps, particularly in the region of the first endotherm, and may reflect the difference in imposed thermal history (slow cooling vs rapid cooling) inherent in the two experiments.

Dielectric Measurements. The measurement of dielectric constant and loss in the range of the liquid-crystalline phase transitions is dominated by Maxwell–Wagner interfacial polarization, particularly at the lower frequencies investigated; this is indicated by the large values of ϵ' and ϵ'' that are observed (Figure 9a). The broad peak that ranges from 130 to 165 °C (10–400 kHz), with a maximum at 145 °C, corresponds to a high degree of local ionic mobility within the sample, with charges trapped at interfacial boundaries. This is most likely due to a mixture of crystalline phases or possibly a mixture of crystalline and smectic phases, as this temperature range extends between the crystal–crystal and crystal-to-smectic A DSC endotherms. Above 145 °C, the number of charge-trapping interphase boundaries diminishes, with an accompanying decrease in the dielectric constant. A similar behavior is observed in the region of smectic A-to-nematic two-phase coexistence, with the creation of a relative maximum at 205 °C.

The higher frequency dielectric measurements (1–10 MHz; Figure 9b) show a far less dramatic behavior and provide some indication of the mobility of the permanent dipole moments along the polymer chains. Specifically, a large incremental increase in dielectric constant is evident in the range of the first (crystal–crystal) DSC endotherm, suggesting the existence of considerable rotational mobility within the "crystalline" network. This mobility is not enhanced across the crystal-to-smectic A transition, the value of ϵ' remaining essentially constant from 130 to 185 °C. At the onset of the nematic phase, ϵ' drops sharply. This result is consistent with a decrease in the order parameter of the rigid mesogenic segments, if one assumes that the polymer chains lie more or less perpendicular to the electric field in the smectic A phase. Such an assumption may, in fact, be valid, considering the compression that is imposed during initial sample preparation, a compression that is likely to align the polymer chains parallel to the electrode surfaces. Further

heating produces a small relative maximum at the nematic–isotropic biphase, with the influence of interfacial polarization now evident even at these high frequencies.

Rheology. The dynamic rheological response of the polymer is highly dependent upon phase state across the successive liquid-crystalline phase transitions. The magnitude of the complex viscosity displays nearly stepwise decreases as a function of increasing temperature at both the crystalline melting and smectic A-to-nematic transitions and a small increase at the onset of isotropy (Figure 11a); this behavior is qualitatively similar to results for other main-chain liquid-crystalline polymers in the literature.[16-18] The rheological response is insensitive, however, to the crystal–crystal transition that occurs in the solid state at 137 °C, despite the large DSC endotherm that is observed at this temperature. Examination of the dynamic moduli over the range 100–160 °C indicates a wholly solidlike behavior ($G' \gg G''$, $G' \neq f(\omega)$; see Figure 15), with the two moduli nearly independent of temperature. In the smectic A phase, the material is highly shear thinning, as is evident from the frequency sweep recorded at 170 °C upon cooling, wherein no (frequency-independent) plateau regions are observed across the measured frequency range (Figure 14); the storage modulus exceeds the loss modulus at this temperature for frequencies up to 100 rad/s. At higher temperatures (>190 °C), the two dynamic modulus–temperature curves coincide (10 rad/s; Figure 11b).

The two sample-loading temperatures that were employed in the course of the rheological experiments (190 and 230 °C) allow an assessment of material stability at high temperature. Specifically, heating to 230 °C has an irreversible effect on the magnitude of the complex viscosity measured in the smectic A phase temperature range, reducing $|\eta^*|$ values by nearly 1 order of magnitude in comparison to those values measured after polymer loading at 190 °C (Figure 12). The values measured in the crystalline, nematic, and isotropic phases are not influenced by loading history. Multiple DSC sweeps, as well as thermogravimetric analysis (TGA), in this upper temperature range do not produce any significant evidence of thermal degradation. One possible explanation for this result is the occurrence of transesterification reactions along the polymer mesogenic segments at high temperature; Kugler et al.[30] observed rapid transesterification reactions for amorphous PET films at similar temperatures (250–280 °C). Such reactions would tend to randomize the length of the mesogenic segments along the polymer chains, and this could reduce the relative amount of smectic ordering that occurs, thus decreasing the magnitude of the complex viscosity measured in the nominally all-smectic A temperature range; these reactions would not necessarily affect the viscosity measured in the isotropic, nematic, or crystalline phases.

Steady shear measurements obtained after sample loading at 230 °C were very sensitive to phase state, despite the possibility of chain randomizations at high temperature. Examination of the steady shear viscosity at a rate of 0.5 s^{-1} upon cooling from 230 °C (Figure 13) suggests a broad nematic–isotropic biphase, with sharp increases in the viscosity at both the nematic-to-smectic A (185 °C) and smectic A-to-crystal (150 °C) phase transitions; below 140 °C the torque limits of the rheometer are exceeded. The steady shear viscosity values measured over the nematic and isotropic phase ranges (above 185 °C) are nearly independent of temperature due to the offsetting combination of increasing isotropic fraction with increasing temperature. This broad biphasic behavior is consistent with our optical and dielectric observations and with ^1H NMR measurements by Amundson,[31] which indicate the persistence of a significant fraction of isotropic material well below the nominal isotropic-to-nematic transition temperature. The increase in viscosity observed below the nematic-to-smectic A transition indicates that the lateral chain interactions of the smectic phase are not destroyed by shearing at a rate of 0.5 s^{-1}, and, in fact, have a dramatic influence on the rheological behavior. Below 150 °C, the material begins to crystallize, thus producing a second increase in viscosity and eventual solidification.

Conclusions

A main-chain thermotropic liquid-crystalline polymer has been characterized by using a variety of methods, with a primary goal of following material rheological behavior over a range of liquid-crystalline phase transitions. Thermal analysis and optical studies reveal that the material displays both a smectic and a nematic mesophase in the melt prior to clearing, consistent with the results of Galli et al.[12] In addition, a sizable DSC endotherm observed at lower temperature (not reported in the work of Galli and co-workers) is found to correspond to a crystal–crystal transition; X-ray diffraction measurements over this range indicate a reorganization of the polymer chains. While the X-ray diffraction measurements are valuable in determining the features of the crystalline phases and the nature of the smectic phase (smectic A), they provide little information with regards to the smectic A-to-nematic transition temperature, the lowest angle (001) reflection showing only a gradual broadening and decrease in intensity upon heating from the smectic to the isotropic state.

Dielectric measurements on the material are largely influenced by ionic conductivity effects but still display a remarkable sensitivity to the observed phase transitions, particularly in regions of two-phase coexistence. At the highest frequencies investigated, the influence of ionic conductivity is relatively small, and the rotational response of the permanent dipoles with temperature can be assessed. A significant increase in dipolar mobility is observed at the crystal–crystal transition, with no perceptible change in dielectric constant across the crystal-to-smectic A transition. At the onset of the nematic phase, a decreasing dielectric constant is encountered, presumably due to a decrease in the overall orientation of the polymer chains.

The melt rheology of the polymer is also highly sensitive to phase state, as measured by both dynamic and steady shear experiments. While no changes in viscosity or modulus can be detected across the crystal–crystal transition (at which temperature the material displays a largely solidlike behavior), distinct discontinuities in the viscosity–temperature curve are evident at temperatures corresponding to the crystal-to-smectic A, smectic A-to-nematic, and nematic-to-isotropic transitions, respectively. Of particular note is the sensitivity of the steady shear viscosity across the smectic A temperature range, which indicates that, at the rate investigated (0.5 s^{-1}), the layering of the smectic A phase is apparently not disrupted by shearing. Dynamic temperature sweeps run from different initial loading temperatures indicate a reduction in the magnitude of the complex viscosity over the smectic A phase temperature range for samples loaded at 230 °C relative to samples loaded at 190 °C. No obvious evidence of polymer degradation is observed at 230 °C, however. It appears possible that transesterification reactions are occurring at the higher loading temperature, partly randomizing the polymer mesogenic segments and reducing

the smectic order parameter or the amount of smectic material present in the nominally all-smectic A temperature range.

Acknowledgment. Work done at the Lawrence Berkeley Laboratory was supported in part by the Director, Office of Energy Research, Office of Basic Energy Sciences, Materials Science Division of the U.S. Department of Energy under Contract No. DE-AC03-76SF00098. D.S.K. was a National Science Foundation Graduate Fellow while at the University of California at Berkeley. P.I. and N.M. were supported by IBM Italy. B. Fuller assisted with the dielectric measurements.

References and Notes

(1) Ober, C. K.; Jin, J.-I.; Lenz, R. W. *Adv. Polym. Sci.* **1984**, *59*, 103.
(2) Blumstein, A.; Asrar, J.; Blumstein, R. B. *Liquid Cryst. Ordered Fluids* **1984**, *4*, 311.
(3) Engel, M.; Hisgen, B.; Keller, R.; Kreuder, W.; Reck, B.; Ringsdorf, H.; Schmidt, H.; Tschirner, P. *Pure Appl. Chem.* **1985**, *57*, 1009.
(4) Shibaev, V. P.; Platé, N. A. *Pure Appl. Chem.* **1985**, *57*, 1589.
(5) Jerman, R. E.; Baird, D. G. *J. Rheol.* **1981**, *25*, 275.
(6) Gotsis, A. D.; Baird, D. G. *J. Rheol.* **1985**, *29*, 539.
(7) Kalika, D. S.; Giles, D. W.; Denn, M. M. *J. Rheol.* **1990**, *34*, 139.
(8) Wissbrun, K. F.; Kiss, G.; Cogswell, F. N. *Chem. Eng. Commun.* **1987**, *53*, 149.
(9) Lin, Y. G.; Winter, H. H. *Macromolecules* **1988**, *21*, 2439.
(10) Lin, Y. G.; Winter, H. H. *Liq. Cryst.* **1988**, *3*, 593.
(11) Kalika, D. S.; Nuel, L.; Denn, M. M. *J. Rheol.* **1989**, *33*, 1059.
(12) Galli, G.; Chiellini, E.; Ober, C. K.; Lenz, R. W. *Makromol. Chem.* **1982**, *183*, 2693.
(13) Porter, R. S.; Johnson, J. F. In *Rheology*; Eirich, F. R., Ed.; Academic Press: New York, 1967; Vol. 4.
(14) Kiss, G.; Porter, R. S. *J. Polym. Sci., Polym. Symp.* **1978**, *65*, 193.
(15) Kiss, G.; Porter, R. S. *J. Polym. Sci., Polym. Phys. Ed.* **1980**, *18*, 361.
(16) Wissbrun, K. F.; Griffin, A. C. *J. Polym. Sci., Polym. Phys. Ed.* **1982**, *20*, 1835.
(17) Blumstein, A.; Thomas, O.; Kumar, S. *J. Polym. Sci., Polym. Phys. Ed.* **1986**, *24*, 27.
(18) Kumar, R. S.; Clough, S. B.; Blumstein, A. *Mol. Cryst. Liq. Cryst.* **1988**, *157*, 387.
(19) Amundson, K. R.; Kalika, D. S.; Shen, M.-R.; Yu, X.-M.; Denn, M. M.; Reimer, J. A. *Mol. Cryst. Liq. Cryst.* **1987**, *153*, 271.
(20) Gedde, U. W.; Buerger, D.; Boyd, R. H. *Macromolecules* **1987**, *20*, 988.
(21) Takase, Y.; Mitchell, G. R.; Odajima, A. *Polym. Commun.* **1986**, *27*, 76.
(22) Blundell, D. J.; Buckingham, K. A. *Polymer* **1985**, *26*, 1623.
(23) Alhaj-Mohammed, M. H.; Davies, G. R.; Abdul Jawad, S.; Ward, I. M. *J. Polym. Sci., Polym. Phys. Ed.* **1988**, *26*, 1751.
(24) Monnerie, L.; Lauprêtre, F.; Noël, C. *Liq. Cryst.* **1988**, *3*, 1013.
(25) Parrish, W. *X-Ray Analysis Papers*; Centrex Publishing Co.: Eindhoven, The Netherlands, 1965.
(26) Huang, T. C.; Parrish, W. *Adv. X-Ray Anal.* **1984**, *27*, 45.
(27) Parrish, W.; Erickson, C. G.; Masciocchi, N., to be submitted for publication.
(28) Bilibin, A. Y.; Tenkovtsev, A. V.; Piraner, O. N.; Pashkovsky, E. E.; Skorokhodov, S. S. *Makromol. Chem.* **1985**, *186*, 1575.
(29) Sironi, A.; Eufri, D. *J. Mol. Graphics*, in press.
(30) Kugler, J.; Gilmer, J. W.; Wiswe, D.; Zachmann, H.-G.; Hahn, K.; Fischer, E. W. *Macromolecules* **1987**, *20*, 1116.
(31) Amundson, K. R. Ph.D. Dissertation, Department of Chemical Engineering, University of California at Berkeley, Berkeley, CA, 1989.
(32) Kalika, D. S.; Yoon, D. Y., submitted for publication in *Macromolecules*.